IJE TRANSACTIONS B: Applications Vol. 33, No. 11, (November 2020) 2408-2415

International Journal of Engineering

Journal Homepage: www.ije.ir

Experimental and Numerical Analysis of Permeability in Porous Media

Z. Sarparast[a], R. Abdoli[b], A. Rahbari[a], M. Varmazyar[a,c], K. Reza Kashyzadeh*[d]

[a] *Department of Mechanical Engineering, Shahid Rajaee Teacher Training University, Tehran, Iran*
[b] *Department of Mechanical Engineering, Islamic Azad University, Damavand Branch, Damavand, Iran*
[c] *Wood Science and Technology Department, Faculty of Civil Engineering, Shahid Rajaee Teacher Training University, Tehran, Iran*
[d] *Department of Mechanical and Instrumental Engineering, Academy of Engineering, Peoples' Friendship University of Russia (RUDN University), 6 Miklukho-Maklaya Street, Moscow, 117198, Russian Federation*

P A P E R I N F O

Paper history:
Received 05 July 2020
Received in revised form 08 August 2020
Accepted 03 September 2020

Keywords:
Tissue Engineering
Porosity
Scaffold
Permeability

A B S T R A C T

Using scaffold microstructure for bone tissue graft has been widely considered. Among the several properties of a scaffold, permeability plays a prominent role in the transport of nutrients, oxygen, and minerals. It is a key parameter which comprises various geometrical features such as pore shape, pore size and interconnectivity, porosity, and specific surface area. The main aim of this research is to characterize the permeability of the scaffold microstructure in terms of different pore sizes and porosity. To this end, cylindrical geometries for pores were modeled and the permeability coefficient was calculated using velocity and pressure drop and employing Darcy's law. The validation process of the numerical results was done by comparing with experimental data. In this regard, a simple experiment setup was presented based on the constant head method. Additionally, the scaffolds were built using Solid Freeform Fabrication (SFF) techniques. The results showed that increasing porosity leads to an increase in permeability. Moreover, the permeability increases as the pore size increases. Eventually, the reducing pore diameters have a significant effect on the flow and hence permeability (e.g., a 20% decrease in diameter yields a 76% decrease in permeability).

***doi**: 10.5829/ije.2020.33.11b.31*

NOMENCLATURE

K	Intrinsic permeability (m^2)	μ	Dynamic fluid viscosity (Pa.s)
$\mathcal{L}$	Specimen thickness (m)	ρ	Density (kg/m^3)
$\mathcal{A}$	Cross-section area (m^2)	V	Velocity (m/s)
$\mathcal{Q}$	Flow rate (m^3/s)	2r	Diameter of the pore (m)
$\Delta\mathcal{P}$	Pressure drop (Pa)	κ	Hydraulic conductivity (m/s)

1. INTRODUCTION

In recent years, significant findings in Bone Tissue Engineering (BTE) have been presented as a result of technological advances. The main purpose of bone graft is to increase the efficiency of the damaged bone. In addition, the bone graft substitutes by incorporating bone progenitor cells are used for specific purposes in different cases (e.g., the healing of bone fractures or between two bones across a diseased joint, to replace and regenerate lost bone due to trauma, infection, or diseases) [1]. Therefore, the use of bone grafts to stimulate the new bone formation is widespread around the world. In this regard, there are three main types of bone grafts called autografts, allografts, and bone graft substitutes. Both autografts and allografts are widely used. However, their limitations lead to use of alternative methods such as bone graft substitutes. A prominent achievement has been made in BTE, in which a highly porous scaffold plays a fundamental role in guiding bone, vascular tissue

*Corresponding Author's Email: *reza-kashi-zade-ka@rudn.ru* (K. Reza Kashyzadeh)

Please cite this article as: Z. Sarparast, R. Abdoli, A. Rahbari, M. Varmazyar, K. Reza Kashyzadeh, Experimental and Numerical Analysis of Permeability in Porous Media, International Journal of Engineering (IJE), IJE TRANSACTIONS B: Applications Vol. 33, No. 11, (November 2020) 2408-2415

growth, and regeneration in three dimensions [2]. In this case, porous scaffolds act as a temporary 3D structure that provides mechanical support for cell migration, cell adhesion, cell proliferation, and finally tissue regeneration [3-8].

Some of the most important features of a suitable scaffold are biocompatibility, biodegradability, and ablity to diffuse cell nutrient and oxygen [9-14]. In addition, different architectural factors, including pore size, pore shape, porosity, and pore interconnectivity affect the efficiency of scaffold [15-18]. In this regard, increasing the pore size (diameter) leads to improve bone formation [19-23]. This result is based on the fact that the enhanced vascularization was observed in larger diameter which provides scaffold with higher oxygen tension and supply of nutrients, conditions that favored direct osteogenesis. Moreover, porosity plays an important role on the osteoconductive properties of the scaffold and the resultant bone tissue ingrowth and vascularization. In this regard, Karageorgiou and Kaplan have stated that higher values of porosity leads to enhance bone ingrowth [21]. In addition, Hollister et al. have investigated the effect of different values of porosity (30, 50, and 70%) in Polypropylene Fumarate/Tri-Calcium Phosphate (PPF/TCP) porous scaffolds [24]. The results of their research showed no significant differences in regenerated bone volume. To response to these conflicting results, a number of scholars have discussed on the permeability as a key parameter to determine scaffold's ability for mass transmission [25-29]. Furthermore, the dependency of permeability on structural parameters including porosity and pore size has been studied by Yang et al. [30]. Besides, Li et al. have proved that the permeability is a specific property of porous materials, which is independent of sample size and the fluid used to measure it [31].

The focus of the present research is on the biomimetic scaffolds and design criteria for their application in bone regeneration. To this end, permeability of the scaffolds was evaluated using simulation of fluid flow within interconnected pores by employing Darcy's law [3, 8, 17-18] in Computational Fluid dynamic (CFD) Analysis. Afterwards, to validate the proposed numerical model, the numerical results were compared with the experiment data obtained by authors. Eventually, by reviewing the literature reported in this paper, the effects of different structural parameters (porosity and pore size) on permeability was investigated using simulations and experiments as an innovation. It is examined quantitatively (not qualitatively) for the first time.

2. MATERIAL AND SPECIMENS

In the present research, the porous scaffolds were designed based on the repetition of a unit cell. A schematic of the designed unit cell in detail is shown in Figure 1. A 3D printer using Solid Free Form (SFF) techniques was used to fabricate the specimens. Six types of scaffolds with different values of structural parameters were provided (Table 1). Figure 2 presents the built specimens of group I.

3. EXPERIMENTAL PROCEDURE

Permeability tests were performed based on Darcy's law which describes the flow of a fluid through a porous media [18].

$$K = \frac{\mu \mathcal{L}}{\mathcal{A}} \frac{Q}{\Delta \mathcal{P}} \quad (1)$$

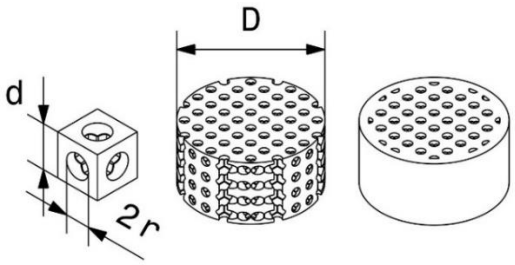

Figure 1. Schematic of the deigned unit cell in detail

TABLE 1. Geometric specifications of the scaffolds manufactured by 3D printing

Parameter	Group I			Group II		
Unit cell (mm)	1.8			2		
Hole diameter (mm)	0.8	1	1.3	0.9	1.1	1.5
Porosity (%)	34	48	70	35	48	72

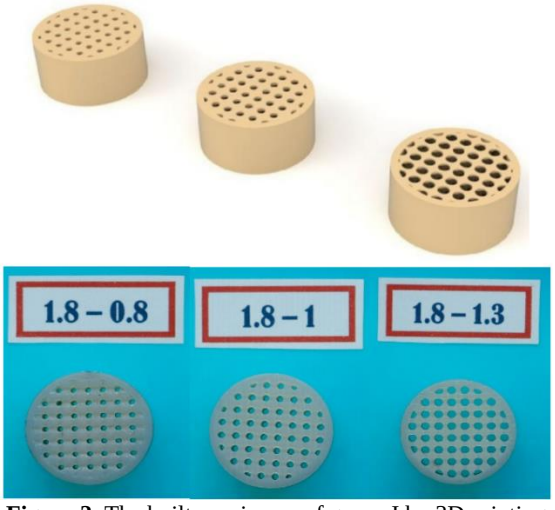

Figure 2. The built specimens of group I by 3D printing

Darcy's law is valid at the low value of Reynolds number, where the flow is laminar and viscous forces are predominant. In practice, Darcy's law is valid for the Reynolds number in the range of 1-10 [32]. In this regard, the Reynolds number is calculated as follows:

$$Re = \frac{\rho V(2r)_{pore}}{\mu} \quad (2)$$

In this study, the geometric parameters of scaffolds including diameter and length are 14 and 8 mm, respectively. Since the permeability is a parameter that is independent of fluid used to measure it and is related to the state of pores interconnectivity [30], water-glycerol at three different values of density and dynamic viscosity (Table 2) was used to fulfill Reynolds number range in Darcy's law.

The permeability measuring device was used to measure the intrinsic permeability as shown in Figure 3. The constant head (gravity-based) permeability test device is composed of an upper reservoir which maintains constant fluid level using fluid flow in and overflow out through separate pipes. Also, a pump has been used to return the overflow fluid from the overflow fluid tank to the fluid storage tank. To perform this test, a fixture with a flexible seating was designed. The most important feature of the designed fixture is that it is able to perform test settings with different scaffolds and various dimensions. The fluid which passes through the scaffold reaches the lower reservoir that is filled with enough amount of fluid to provide constant fluid level. Therefore, as soon as the fluid reaches the lower reservoir overflows to a collector seated on an electronic scale (EK-300i AND weighing), the mass flow rates of the fluid are recorded consecutively by having the weight of the fluid in any particular time points. Afterwards, the data are sent to Win CT program for computer analyzing. As a result, the average mass flow rate is calculable through a period of time. Finally, the average mass flow rate is substituted in Equation (3) to calculate permeability coefficient of the porous scaffold. Three measurements for each scaffold specimen were conducted to ensure the repeatability of test results.

$$K = \kappa \frac{\mu}{\rho g} \quad (3)$$

4. NUMERICAL SIMULATION

In the present research, SolidWorks as one of the well-known Computed Aided Design (CAD) software was used to prepare the geometric model. In this regard, six different 3D models were designed according to Table 1.

TABLE 2. Values of density and dynamic viscosity of water-glycerol

Water-glycerol Properties	
μ (pa-s)	ρ (kg/m³)
0.01	1158.7
0.0183	1179.5
0.047	1207

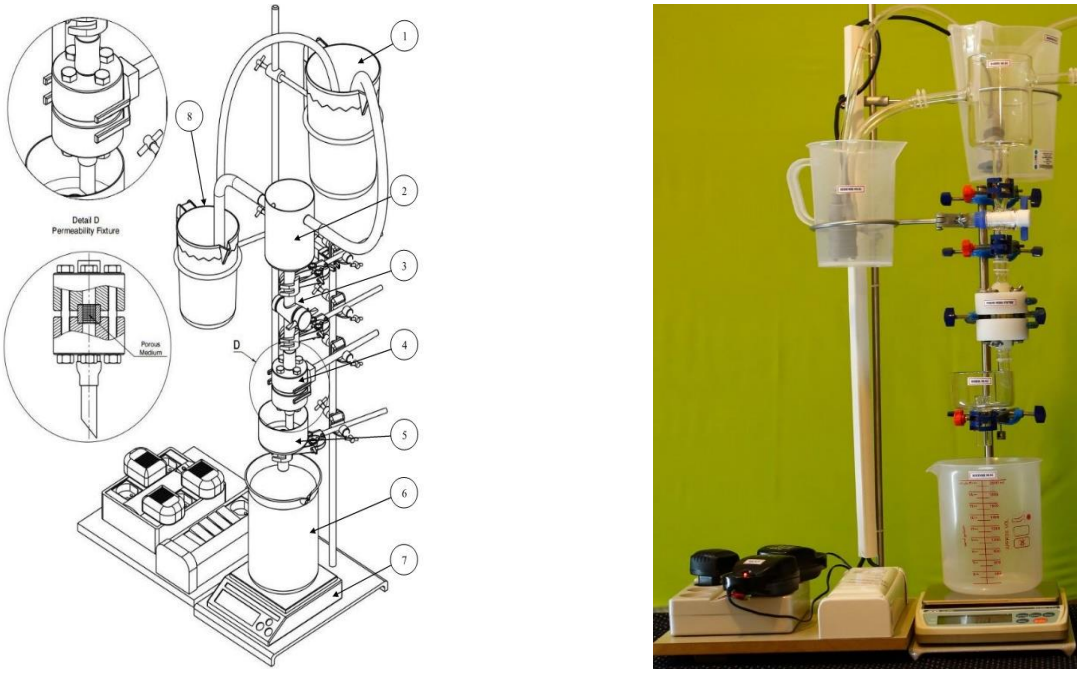

Figure 3. The 3D model of designed constant head permeability test setup, (1) Fluid storage tank, (2) Upper reservoir, (3) Valve, (4) Fixture, (5) Lower reservoir, (6) Collector, (7) Electronic scale, (8) Overflow fluid tank.

Furthermore, various modules of ANSYS 16.0 (i.e., ANSYS ICEM CFD, CFD packages, and ANSYS Fluent) were used to mesh the model, create Finite Volume Method (FVM), apply boundary conditions, and solve the problem.

The tetrahedral adaptation scheme (code 3D_TAG) was used based on the Biswas and Strawn statement [33]. In addition, mesh refinement was done by the first setting because the repeated refinement can lead to poor quality of mesh and affect the accuracy of the response. Moreover, mesh response sensitivity analysis was also performed to reduce computational costs and to determine the best parameters in the first setting such as element size [34-36]. Eventually, 100,000-600,000 tetrahedral meshes were generated on the designed scaffolds (the number of meshes depends on the scaffold sizes). Figure 4 illustrates the mesh model of one of the designed scaffolds as a representative.

The flow was simulated to study the mass flow rate, flow velocity, and flow pressure in scaffolds. To this end, a pressure-based solver and laminar, Newtonian, constant temperature, incompressible and homogeneous flow, inlet velocity between 0.03 m/s and 0.15 m/s, and outlet pressure of zero Pascal were assumed as boundary conditions. The schematic of inlet and outlet of fluid flow within the scaffolds is demonstrated in Figure 5. The equations of conservation of mass and momentum (Equation (4)) and continuity (Equation (5)) were used in this simulation. Finally, the permeability of scaffolds was computed based on Darcy's law.

$$\rho(V.\nabla V) = -\nabla P + \mu\nabla^2 V + \rho g \quad (4)$$

$$\varphi\frac{\partial\rho}{\partial t} + \nabla.(\rho V) = 0 \quad (5)$$

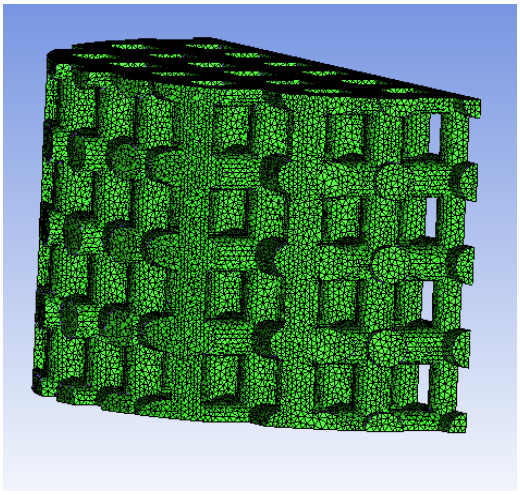

Figure 4. The mesh model of one of the designed scaffolds as a representative

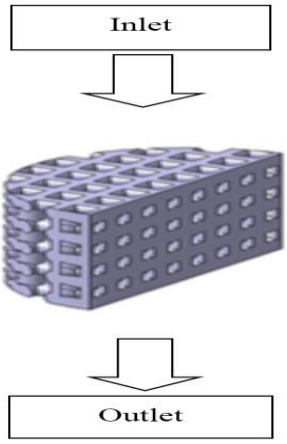

Figure 5. The schematic of inlet and outlet of fluid flow within the scaffolds used in ANSYS Fluent.

5. RESULTS AND DISCUSSION

5. 1. Numerical Results Numerical permeability coefficient values in terms of various porosity as a result of CFD analysis within an interval of (5.009-41.826) $\times 10^{-9}$ are presented in Figure 6. The contour maps in Figure 7 illustrate the range of velocities across the scaffold with unit cell size of 2mm and porosity of 70% and 35% for the longitudinal plane with the greatest flow rate at the center of the cylindrical pore.

The reliability of CFD calculations for predicting permeability of tissue engineering scaffolds were assessed with regards to computational data presented by Dias et al. [3]. Figure 8 presents the comparison of the numerical results obtained in this research and the Dias model.

5. 2. Experimental Results Figure 9 presents a comparison between the numerical results obtained in

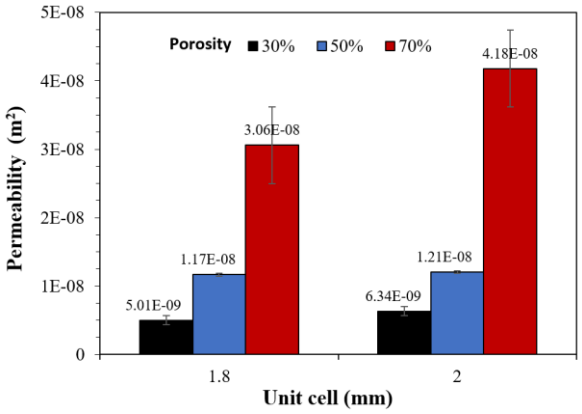

Figure 6. Numerical permeability coefficient values in terms of various porosity for different size of unit cell

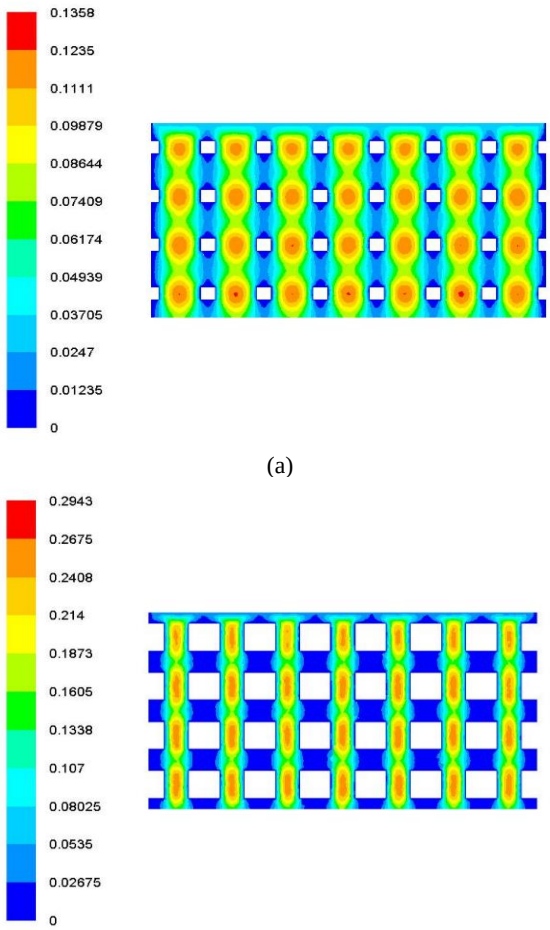

Figure 7. Velocity contour of the scaffold with unit cell size 2mm and different porosity including a) 70% and b) 30%

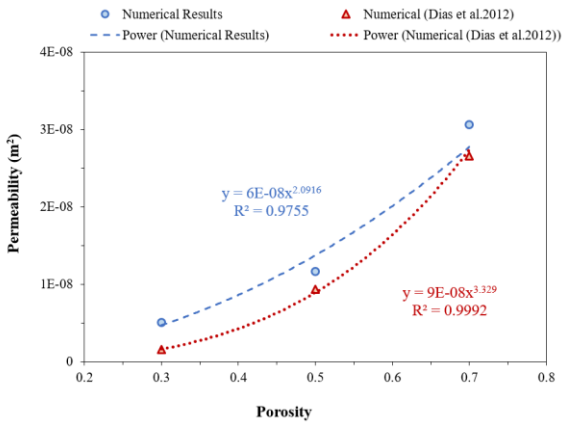

Figure 8. Comparison of permeability values versus porosity for scaffold with unit cell 1.8mm between present numerical model and Dias et al. model

this study and the experimental results for different cases of designed scaffolds. Both experiment and numerical methods show the same trend for permeability versus porosity; increasing porosity leads to an increase in permeability. Moreover, the proposed numerical model also predicts the permeability values more than the real values (experimental data). The results indicated that the accuracy of presented numerical model decreases by raising porosity. In other words, the difference between the numerical and test results in porosity of 70 and 30% is the highest and lowest value, respectively.

5. 3. Effect of Pore Size The experimental data obtained in the previous section were used to examine the geometric effect of the design. Therefore, the influence of the pore size on the permeability is depicted in Figure 10. It is clear that the permeability increases as the pore size increases. Moreover, reducing pore diameters have a significant effect on the flow and hence permeability (e.g., 20% decrease in diameter yields a 76% decrease in permeability).

Next, the numerical results were compared with the experimental values (Figure 11). A linear relationship is obtained using regression method with R^2=0.9605, which indicates a good correlation between the numerical and the experimental data.

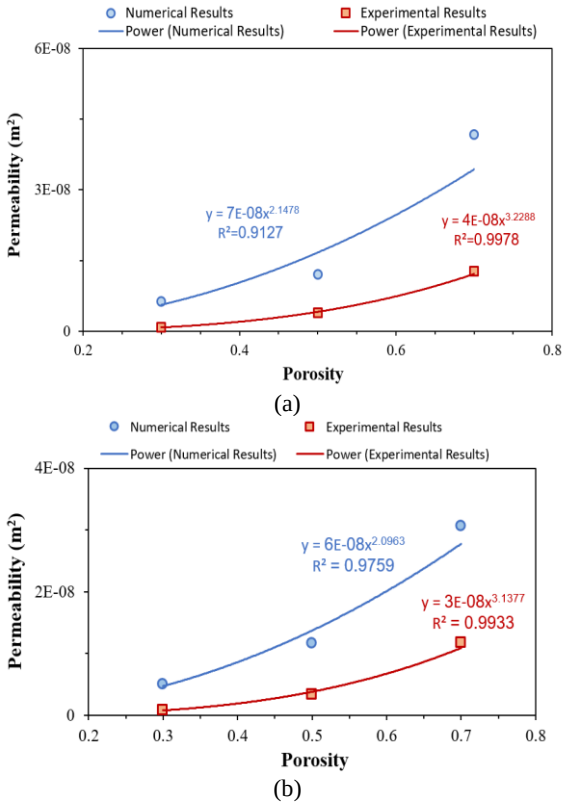

Figure 9. The relationship between permeability and porosity of designed scaffolds with a comparison of numerical and experimental results for different unit cell sizes: a) 2 mm and b) 1.8 mm

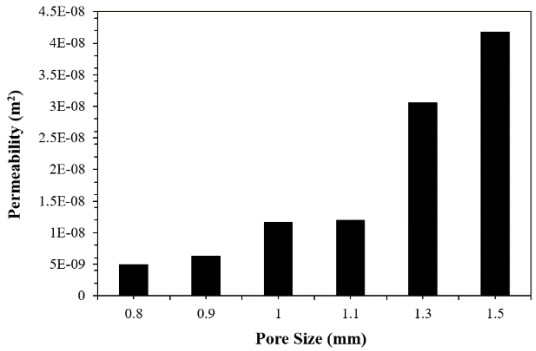

Figure 10. The impact of pore size on the permeability of designed scaffolds

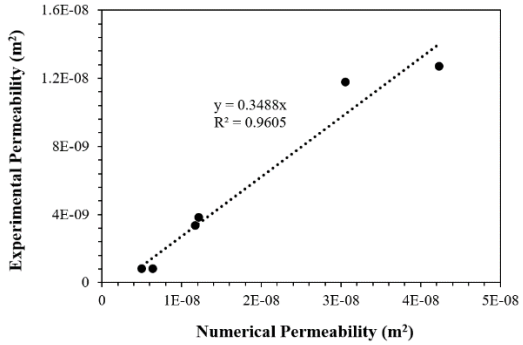

Figure 11. Relationship of experimental vs. numerical results

For a single hole, Hagen-Poiseuille equation described the pressure drop (Δp) through a cylindrical pipe as:

$$\Delta p = \frac{8Q\mu L}{\pi r^4} \quad (6)$$

By replacing Hagen-Poiseuille equation in Darcy's law it is possible to the inference that permeability is proportional to the square of pore radius. Therefore, in this study, we can assume that:

$$K = \alpha \frac{r^2}{8} \quad (7)$$

By depicting experimental values versus numerical ones a linear relationship between data can be observed, according to Figure 11, this relation leads to a coefficient α=0.3488. In this regard, other researchers have similarly extracted the alpha coefficient [3, 29, 37-38]. In this respect, an adjustment should be proposed to the numerical values with the α coefficient. Permeability results after this fitting are demonstrated in Figure 12.

Given the fact that experimental results are smaller than numerical ones probably due to ignorance of reverse flow and surface effects such as wettability and roughness. Although, we considered laminar flow in the experimental procedure by utilizing water-glycerol to maintain Reynolds number between one and 10.

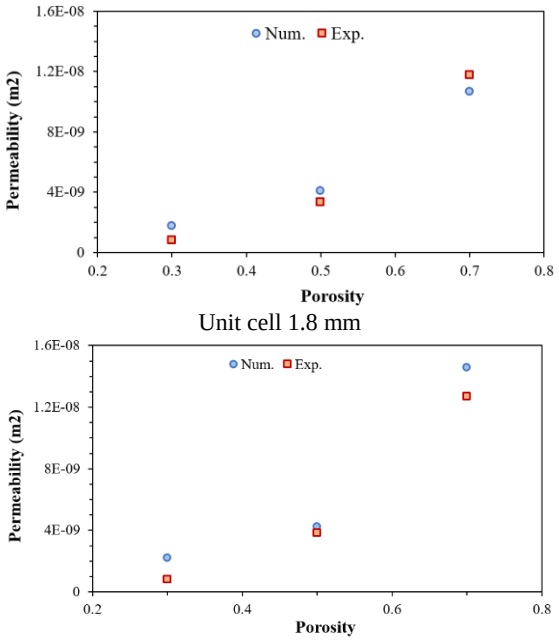

Figure 12. The relationship between permeability and porosity in the field of numerical and experimental results with consideration of the α coefficient

6. CONCLUSION

This study presents a design tool to investigate the effect of differences between design specifications and actual manufactured geometries on permeability to make it possible to predict permeability values numerically for porous materials with a certain design. Furthermore, it provides a criterion to predict permeability of scaffolds in terms of porosity for specific geometries to reduce the number of experimental studies necessary to validate design performance. In addition, it can be observed that permeability is a function of porosity and pore size. The main achievement of this research reveal that with the same porosity, higher permeability value can be achieved by only increasing pore size provided that mechanical properties were maintained in a bigger unit cell size.

7. ACKNOWLEDGMENTS

The publication has been prepared with the support of the "RUDN University Program 5-100".

8. REFERENCES

1. Polo-Corrales. L, Latorre-Esteves. M, and Ramirez-Vick. J. E, "Scaffold design for bone regeneration", ***Journal of Nanoscience and Nanotechnology***, Vol. 14, No. 1, (2014), 15-56, DOI: 10.1166/jnn.2014.9127

2. Thavornyutikarn. B, Chantarapanich. N, Sitthiseripratip. K, Thouas. G. A, and Chen. Q, "Bone tissue engineering scaffolding: computer-aided scaffolding techniques", ***Progress in Biomaterials.***, Vol. 3, (2014), 61-102, DOI: 10.1007/s40204-014-0026-7
3. Dias. M. R, Fernandes. P. R, Guedes. J. M, and Hollister. S. J, "Permeability analysis of scaffolds for bone tissue engineering", ***Journal of Biomechanics***, Vol. 45, No. 6, (2012), 938-944, DOI: 10.1016/j.jbiomech.2012.01.019
4. Chan. G, and Mooney. D. J, "New materials for tissue engineering: towards greater control over the biological response", ***Trends in Biotechnology***, Vol. 26, No. 7, (2008), 382-392, DOI: 10.1016/j.tibtech.2008.03.011
5. Lemon. G, Reinwald. Y, White. L. J, Howdle. S. M, Shakesheff. K. M, and King. J. R, "Interconnectivity analysis of supercritical CO2-foamed scaffolds", ***Computer Methods and Programs in Biomedicine***, Vol. 106, No. 3, (2012), 139-149, DOI: 10.1016/j.cmpb.2010.08.010
6. Ochoa. I, Sanz-Herrera. J. A, García-Aznar. J. M, Doblaré. M, Yunos. D. M, and Boccaccini. A. R, "Permeability evaluation of 45S5 Bioglass®-based scaffolds for bone tissue engineering", ***Journal of Biomechanics***, Vol. 42, No. 3, (2009), 257-260, DOI: 10.1016/j.jbiomech.2008.10.030
7. Reinwald. Y, Johal. R. K, Ghaemmaghami. A. M, Rose. F. R. A. J, Howdle. S. M, and Shakesheff. K. M, "Interconnectivity and permeability of supercritical fluid-foamed scaffolds and the effect of their structural properties on cell distribution", ***Polymer***, Vol. 55, No. 1, (2014), 435-444, DOI: 10.1016/j.polymer.2013.09.041
8. Viana. T, Biscaia. S, Almeida. H. A, and Bártolo. P. J, "Permeability evaluation of lay-down patterns and pore size of PCL scaffolds", ***Procedia Engineering***, Vol. 59, (2013), 255-262, DOI: 10.1016/j.proeng.2013.05.119
9. Botchwey. E. A, Dupree. M. A, Pollack. S. R, Levine. E. M, and Laurencin. C. T, "Tissue engineered bone: Measurement of nutrient transport in three-dimensional matrices", ***Journal of Biomedical Materials Research Part A: An Official Journal of the Society for Biomaterials,*** The Japanese Society for Biomaterials, and The Australian Society for Biomaterials and the Korean Society for Biomaterials, Vol. 67, No. 1, (2003), 357-367, DOI: 10.1002/jbm.a.10111
10. Chan. B. P, and Leong. K. W, "Scaffolding in tissue engineering: general approaches and tissue-specific considerations", ***European Spine Journal***, Vol. 17, No. 4, (2008), 467-479, DOI: 10.1007/s00586-008-0745-3
11. Pennella. F, Cerino. G, Massai. D, Gallo. D, Labate. G. F. D. U, Schiavi. A, Deriu. M. A, Audenino. A, and Morbiducci. U, "A survey of methods for the evaluation of tissue engineering scaffold permeability", ***Annals of Biomedical Engineering***, Vol. 41, No. 10, (2013), 2027-2041, DOI: 10.1007/s10439-013-0815-5
12. Rakovsky. A, Gotman. I, Rabkin. E, and Gutmanas. E. Y, "β-TCP–polylactide composite scaffolds with high strength and enhanced permeability prepared by a modified salt leaching method", ***Journal of the Mechanical Behavior of Biomedical Materials***, Vol. 32, (2014), 89-98, DOI: 10.1016/j.jmbbm.2013.12.022
13. Serpooshan. V, Quinn. T. M, Muja. N, and Nazhat. S. N, "Hydraulic permeability of multilayered collagen gel scaffolds under plastic compression-induced unidirectional fluid flow", ***Acta Biomaterialia***, Vol. 9, No. 1, (2013), 4673-4680, DOI: 10.1016/j.actbio.2012.08.031
14. Sharma. B, and Elisseeff. J. H, "Engineering structurally organized cartilage and bone tissues", ***Annals of Biomedical Engineering***, Vol. 32, No. 1, (2004), 148-159, DOI: 10.1023/B:ABME.0000007799.60142.78
15. Amirkhani. S, Bagheri. R, and Yazdi. A. Z, "Effect of pore geometry and loading direction on deformation mechanism of rapid prototyped scaffolds", ***Acta Materialia***, Vol. 60, No. 6-7, (2012), 2778-2789, DOI: 10.1016/j.actamat.2012.01.044
16. Hollister. S. J, "Porous scaffold design for tissue engineering", ***Nature Materials***, Vol. 4, No. 7, (2005), 518-524, DOI: 10.1038/nmat1421
17. Syahrom. A, Kadir. M. R. A, Abdullah. J, and Öchsner. A, "Permeability studies of artificial and natural cancellous bone structures", ***Medical Engineering & Physics***, Vol. 35, No. 6, (2013), 792-799, DOI: 10.1016/j.medengphy.2012.08.011
18. Truscello. S, Kerckhofs. G, Van Bael. S, Pyka. G, Schrooten. J, and Van Oosterwyck. H, "Prediction of permeability of regular scaffolds for skeletal tissue engineering: a combined computational and experimental study", ***Acta Biomaterialia***, Vol. 8, No. 4, (2012), 1648-1658, DOI: 10.1016/j.actbio.2011.12.021
19. Gross. K. A, and Rodríguez-Lorenzo. L. M, "Biodegradable composite scaffolds with an interconnected spherical network for bone tissue engineering", ***Biomaterials***, Vol. 25, No. 20, (2004), 4955-4962, DOI: 10.1016/j.biomaterials.2004.01.046
20. Hutmacher. D. W, Schantz. J. T, Lam. C. X. F, Tan. K. C, and Lim. T. C., "State of the art and future directions of scaffold-based bone engineering from a biomaterials perspective", ***Journal of Tissue Engineering and Regenerative Medicine***, Vol. 1, No. 4, (2007), 245-260, DOI: 10.1002/term.24
21. Karageorgiou. V, and Kaplan. D, "Porosity of 3D biomaterial scaffolds and osteogenesis", ***Biomaterials***, Vol. 26, No. 27, (2005), 5474-5491, DOI: 10.1016/j.biomaterials.2005.02.002
22. Murphy. C. M, Haugh. M. G, and O'brien. F. J, "The effect of mean pore size on cell attachment, proliferation and migration in collagen–glycosaminoglycan scaffolds for bone tissue engineering", ***Biomaterials***, Vol. 31, No. 3, (2010), 461-466, DOI: 10.1016/j.biomaterials.2009.09.063
23. O'Brien. F. J, Harley. B. A, Yannas. I. V, and Gibson. L. J, "The effect of pore size on cell adhesion in collagen-GAG scaffolds", ***Biomaterials***, Vol. 26, No. 4, (2005), 433-441, DOI: 10.1016/j.biomaterials.2004.02.052
24. Hollister. S. J, Liao. E. E, Moffitt. E. N, Jeong. C. G, and Kemppainen. J. M, "Defining design targets for tissue engineering scaffolds", ***In Fundamentals of Tissue Engineering and Regenerative Medicine***, (2009), 521-537, DOI: 10.1007/978-3-540-77755-7_38
25. Grimm. M. J, and Williams. J. L, "Measurements of permeability in human calcaneal trabecular bone", ***Journal of Biomechanics***, Vol. 30, No. 7, (1997), 743-745, DOI: 10.1016/S0021-9290(97)00016-X
26. Jones. A. C, Arns. C. H, Hutmacher. D. W, Milthorpe. B. K, Sheppard. A. P, and Knackstedt. M. A, "The correlation of pore morphology, interconnectivity and physical properties of 3D ceramic scaffolds with bone ingrowth", ***Biomaterials***, Vol. 30, No. 7, (2009), 1440-1451, DOI: 10.1016/j.biomaterials.2008.10.056
27. Mitsak. A. G, Kemppainen. J. M, Harris. M. T, and Hollister. S. J, "Effect of polycaprolactone scaffold permeability on bone regeneration in vivo", ***Tissue Engineering Part A***, Vol. 17, No. 13-14, (2011), 1831-1839, DOI: 10.1089/ten.tea.2010.0560
28. Sandino. C, Kroliczek. P, McErlain. D. D, and Boyd. S. K, "Predicting the permeability of trabecular bone by micro-computed tomography and finite element modeling", ***Journal of Biomechanics***, Vol. 47, No. 12, (2014), 3129-3134, DOI: 10.1016/j.jbiomech.2014.06.024
29. Sell. S, Barnes. C, Simpson. D, and Bowlin. G, "Scaffold permeability as a means to determine fiber diameter and pore size of electrospun fibrinogen", ***Journal of Biomedical Materials Research Part A: An Official Journal of the Society for Biomaterials***, The Japanese Society for Biomaterials, and the Australian Society for Biomaterials and the Korean Society for Biomaterials, Vol. 85, No. 1, (2008), 115-126, DOI: 10.1002/jbm.a.31556

30. Yang. X, Lu. T. J, and Kim. T, "An analytical model for permeability of isotropic porous media", ***Physics Letters A***, Vol. 378, No. 30-31, (2014), 2308-2311, DOI: 10.1016/j.physleta.2014.06.002

31. Li. S, de Wijn. J. R, Li. J, Layrolle. P, and de Groot. K, "Macroporous biphasic calcium phosphate scaffold with high permeability/porosity ratio", ***Tissue Engineering***, Vol. 9, Issue. 3, (2003), 535-548, DOI: 10.1089/107632703322066714

32. Bear. J, "Dynamics of fluids in porous media", Courier Corporation, (2013), ISBN-13: 978-0-486-65675-5

33. Biswas. R, and Strawn. R. C, "Tetrahedral and hexahedral mesh adaptation for CFD problems", ***Applied Numerical Mathematics***, Vol. 26, No. 1-2, (1998), 135-151, DOI: 10.1016/S0168-9274(97)00092-5

34. Reza Kashyzadeh. K, Farrahi. G. H, Shariyat. M, and Ahmadian. M. T, "Experimental and finite element studies on free vibration of automotive steering knuckle", ***International Journal of Engineering. Transaction B: Applications***, Vol. 30, No. 11, (2017), 1776-1783, DOI: 10.5829/ije.2017.30.11b.20

35. Reza Kashyzadeh. K, "Effects of axial and multiaxial variable amplitude loading conditions on the fatigue life assessment of automotive steering knuckle", ***Journal of Failure Analysis and Prevention***, Vol. 20, (2020), 455-463, DOI: 10.1007/s11668-020-00841-w

36. Farrahi. G. H, Reza Kashyzadeh. K, Minaei. M, Sharifpour. A, and Riazi. S, "Analysis of resistance spot welding process parameters effect on the weld quality of three-steel sheets used in automotive industry: experimental and finite element simulation", ***International Journal of Engineering. Transaction A: Basics***, Vol. 33, No. 1, (2020), 148-157, DOI: 10.5829/ije.2020.33.01a.17

37. Andersson. L, Jones. A. C, Knackstedt. M. A, and Bergström. L, "Permeability, pore connectivity and critical pore throat control of expandable polymeric sphere templated macroporous alumina", ***Acta Materialia***, Vol. 59, No. 3, (2011), 1239-1248, DOI: 10.1016/j.actamat.2010.10.056

38. O'Brien. F. J, Harley. B. A, Waller. M. A, Yannas. I. V, Gibson. L. J, and Prendergast. P. J, "The effect of pore size on permeability and cell attachment in collagen scaffolds for tissue engineering", ***Technology and Health Care***, Vol. 15, No. 1, (2007), 3-17, DOI: 10.3233/THC-2007-15102

Persian Abstract

چکیده

استفاده از داربست‌های ریزساختار برای پیوند بافت استخوان به طور گسترده‌ای مورد توجه قرار گرفته است. در میان ویژگی‌های داربست، نفوذپذیری نقش مهمی در انتقال مواد مغذی، اکسیژن و مواد معدنی دارد. این یک پارامتر کلیدی است که شامل ویژگی‌های مختلف هندسی مانند شکل و اندازه منافذ و اتصال متقابل، تخلخل و مساحت ویژه است. هدف اصلی این پژوهش توصیف نفوذپذیری داربست‌های ریزساختار از نظر اندازه‌ی منافذ مختلف و تخلخل است. برای این منظور، منافذ با هندسه‌های استوانه‌ای شکل مدل شده و با استفاده از مقادیر سرعت و افت فشار و با به‌کارگیری قانون دارسی ضریب نفوذپذیری محاسبه شد. فرایند اعتبارسنجی نتایج عددی با مقایسه با داده‌های تجربی انجام شد. در این راستا، یک آزمایش ساده بر اساس روش سر ثابت ارائه شد. داربست‌ها با استفاده از فنون ساخت جامد فرم-آزاد (SFF) ساخته شدند. نتایج نشان داد که افزایش تخلخل منجر به افزایش نفوذپذیری می‌شود. علاوه بر این، با افزایش اندازه‌ی منافذ، نفوذپذیری نیز افزایش می‌یابد. در نهایت، کاهش قطر منافذ تأثیر قابل توجهی بر جریان، و در پی آن نفوذپذیری دارد (به عنوان مثال، کاهش ۲۰ درصدی قطر منجر به کاهش ۷۶ درصدی نفوذپذیری می‌شود).